



Evaluation of high-resolution and depth-encoding PET detector modules based on single-ended readout with TOFPET2 ASIC

Mingchen Wang¹ · Yonggang Wang¹ · Liwei Wang¹

Received: 26 April 2021 / Revised: 8 June 2021 / Accepted: 22 June 2021 / Published online: 6 July 2021
© Institute of High Energy Physics, Chinese Academy of Sciences 2021

Abstract

Purpose We developed a low-complexity, high-resolution depth-of-interaction (DOI) capable positron emission tomography (PET) detector and tested its performance to prove that it can be applied to practical PET instruments.

Methods The detector module consists of a 24×24 LYSO crystal matrix, each with dimension of $1.04 \times 1.04 \times 15 \text{ mm}^3$, optically coupled to an 8×8 SiPM photo-sensor array with TOFPET2 ASIC single-ended readout. By only adding a light guide at the top of the crystal to reflect scintillation light back to the SiPM array, the continuous DOI information is extracted using a light sharing and redirection encoding method without adding system complexity.

Results The crystal array with 9-to-1 coupling between scintillators and photo-sensors can be clearly separated in the flood image. The other detector performance in terms of DOI resolution, energy resolution and coincidence time resolution are measured on average as 4.1 mm, 15.0% and 432 ps, respectively.

Conclusion The test results confirm that the light sharing and redirection DOI encoding method can provide reasonably high DOI resolution without deteriorating other performance, even for highly pixelated PET detectors readout with commercially available ASIC chip. It has great potential for applications in future pre-clinical and organ-dedicated PET scanners.

Keywords High-resolution · Depth-of-interaction · TOFPET2 ASIC · PET detector

Introduction

Spatial resolution and sensitivity are two important performances in PET system [1, 2]. In particular, for current pre-clinical and organ-dedicated human PET scanners, very high levels of spatial resolution, typically in the order of 1 mm are required. The high spatial resolution is usually achieved by developing detectors using scintillators with small cross section and arranging detectors in a ring with small diameter [3, 4, 5]. Meanwhile, the sensitivity is usually improved by using long crystal and long axial field of view. Since the spatial resolution will be degraded if traditional non-depth encoding PET detectors are used due to the DOI uncertainty or parallax error [6], developing of high spatial resolution PET detectors with DOI capability has become a key research area in PET instrumentation.

Among a large number of feasibility studies to achieve high performance for PET detectors, low system complexity and low production cost must be considered for practical PET instrumentation. Achieving high spatial resolution by reducing the transverse dimension of scintillators may greatly increase the number of detector readout channels, in particular if a one-to-one coupling between crystals and photo-sensors is adopted. The popular solution to reduce this readout burden is coupling multiple crystals to one photo-sensor active area. By spreading the scintillation light into adjacent detector channels, the hit crystal can be identified with angle formula [7]. There is a compromise between the coupling ratio and crystal identification, which can be achieved relying on the quality of measured flood image of detector. To have DOI information to improve the trade-off between sensitivity and spatial resolution, various DOI encoding techniques have been studied in recent years including dual-ended readout scintillator arrays [8], multi-layer crystals [9], and inter-crystal reflector arrangements [10]. Although the dual-ended readout method has advantages of high spatial resolution and DOI resolution, the main

✉ Yonggang Wang
wangyg@ustc.edu.cn

¹ Modern Physics Department, University of Science and Technology of China, Hefei 230026, Anhui, China

drawbacks of these methods are the high system complexity and hence the production cost.

In comparison, the newly proposed light sharing and redirection DOI encoding method [11, 12] can obtain reasonably high performance, at the same time keeping the complexity of system low. Based on the normal single-ended readout pixelated PET detector, by adding only a piece of light guide on the top of crystal array to reflect the scintillation light toward the top end back to the photo-sensors, the DOI information can be estimated using the light sharing technique. The authors constructed the prototype detector using a single-ended readout and 4-to-1 coupling ratio between LYSO crystals and a commercial SiPM array. The mean DOI resolution of 4.1 mm FWHM on a 15 mm long crystal was achieved without obvious loss of other properties in terms of crystal identification, energy resolution, and the timing resolution. The authors also further demonstrated that the light sharing and redirection scheme they proposed does not degrade the timing performance of the PET detector module [13].

In this paper, we are developing a high-resolution DOI capable PET detector based on the light sharing and redirection method toward practical PET instrumentation. The first difference from the previous work is the 9-to-1 coupling ratio between the LYSO crystals and SiPM photo-sensors, therefore, the spatial resolution will be pushed down to 1.0 mm without adding readout complexity. The second difference is that we use commercialized 64-channel readout ASIC chip, TOFPET2 from PETsys (Oeiras, Portugal) [14, 15], to construct the detector module instead of using the acquisition system consisting of specially designed circuit board connected to desktop standard digitizer module in [11, 12]. The aim of our work is to evaluate the achievable performance of the detector module with the method under current existing engineering conditions, which is necessary preparation for our next PET system construction. The evaluation results confirm that the DOI encoding method is still effective even for highly pixelated PET detectors readout with commercially available ASIC chip. Its high performance and low system complexity show that it is very practical for applications in future pre-clinic and organ-dedicated PET scanners.

Materials and Methods

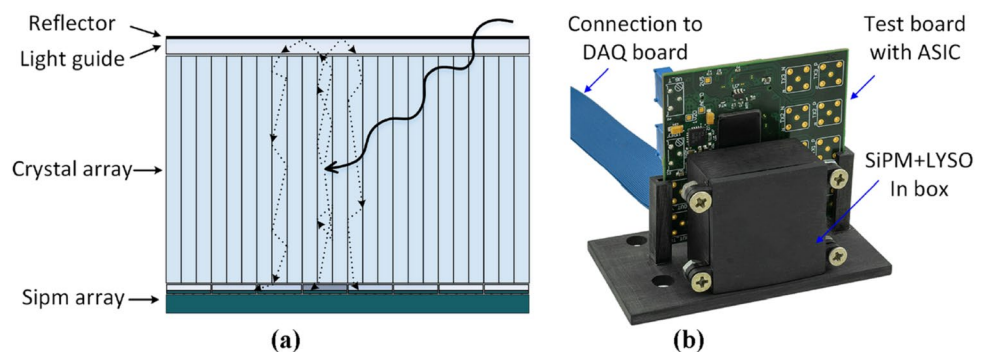
Detector module

The detector is composed of an 8×8 SiPM array (KETEK PA3325-WB-0808), a 24×24 LYSO crystal matrix (Epic crystal Co., Ltd) and a block of light guide ($27 \times 27 \times 1 \text{ mm}^3$ K-9 glass) as shown in Fig. 1a. One side of the crystal is coupled to the SiPM array by optical grease, and the other side is covered with the light guide of a layer of Enhanced Specular Reflector (ESR). Each channel of the SiPM array has an active area of $3 \times 3 \text{ mm}^2$ with a pitch of 3.36 mm, and each element of the crystal matrix has dimensions of $1.04 \times 1.04 \times 15 \text{ mm}^3$. The top and bottom surface of each crystal are polished, while the lateral surfaces are de-polished. The crystals are separated by a layer of $70 \text{ }\mu\text{m}$ thick ESR. Taking the thickness of separation in between the crystals into account, the outline dimension of the crystal array is exactly the same as that of the SiPM array.

The signals from the SiPM array are measured with a TOFPET2 ASIC, which is a low power ASIC chip with 64 channels optimized for readout of SiPM for time-of-flight PET applications. Every readout channel in the chip works independently, which uses a low threshold for timing and a high threshold for event validation. Every time one of the 64 channels exceeds the high threshold, a record is created giving out the channel number, the time and the charge of the event. Activity in one channel does not cause any dead-time on other channels. Based on the ASIC test board provided in the evaluation kit by PETsys, our detector module is constructed as shown in Fig. 1b. The SiPM array is plugged directly into the test board, which integrates TOFPET2 ASIC allowing the readout of 64 SiPM channels and transmission to a dedicated data acquisition board through the flat cable. The whole detector is housed in a black plastic light-shielding box.

Using the on-board thermometer in the test board, the ambient temperature can be monitored in real time. The temperature of the chip was measured as $28 \pm 1 \text{ }^\circ\text{C}$ during

Fig. 1 Composition of **a** the detector and **b** the detector module



the whole evaluation process. The energy window used for flood images and DOI resolution is 350–700 keV. But when acquiring time performance, only events within the FWHM of the energy photopeak are selected. The over-voltage of the SiPM is 5 V, and the three thresholds T1, T2, and E in PETsys are, respectively, set to 20, 12 and 12.

Readout energy calibration

In the detectors with multiple crystals coupled to one photo-sensor active area, the hit crystal is identified by the light sharing detected by multiple channels nearby and calculated with Anger formula. Therefore, the energy calibration for all the readout channels is necessary, in particular for highly pixelated detectors with a high coupling ratio between crystals and photo-sensors. In addition, the DOI encoding method used in this paper is also relying on the scintillation light sharing, which makes the energy calibration more crucial.

The purpose of energy calibration is to obtain the transfer function between the deposited energy and the output number of TOFPET2 (i.e., QDC number in arbitrary unit), so that the readouts from different channels after calibration are comparable. In our previous work [16], we have developed a relatively simple energy calibration method using the background radiation of LYSO crystal. Using the radiation of the isotope ¹⁷⁶Lu in LYSO crystal and an external ²²Na source, we can acquire an energy spectrum with four energy peaks as shown in Fig. 2 for each readout channel that can be used for calibration.

According to the theoretical analysis in [17], the transfer function of each readout channel can be simply expressed as:

$$QDC = K_1(1 - e^{-K_2E}) + b_0 \tag{1}$$

where, b_0 represents the offset of the channel, K_1 is the transfer coefficient from the fired microcells to the QDC number, E is the energy deposited in the channel, and K_2

represents the difference of response to the deposited energy E in the channel.

Using the measured four energy peaks in Fig. 2 to fit Eq. (1), the three parameters K_1 , K_2 , and b_0 can be obtained, and the transfer function for the channel is determined. Through the transfer function, the readout QDC number in each channel can be translated into a correct energy value.

Plane (x, y) and DOI determination

The principle of the DOI method is based on light sharing and redirection together with the attenuation of light along the length of the crystals as shown in Fig. 1. The photons produced by the interact of a gamma ray with a crystal propagate through the crystal, some exit from the coupled side to SiPM, and the others are redirected to the surrounding channels by the light guide with reflector on the opposite side. The energy ratio w depends on the depth of interaction z , moreover, the previous experimental results show that w and z are linearly dependent [11]. Multiple SiPM channels will be fired for one interaction, therefore, the plane coordinates (x, y) is computed by the Anger logic (2), and the DOI is determined by charge distribution calculated with (3) and (4).

$$x = \frac{1}{P} \sum_i^N p_i x_i \quad y = \frac{1}{P} \sum_i^N p_i y_i \quad P = \sum_i^N p_i \tag{2}$$

$$w = \frac{P_{max}}{P} \tag{3}$$

$$z = k \cdot w + b \tag{4}$$

$$\sigma(z) = k \cdot \sigma(w) \tag{5}$$

where, x_i , y_i and p_i are the positions and collected charge of the i -th SiPM, and P_{max} is the maximum energy measured by all SiPMs. Parameters k and b in (4) will be determined by the DOI calibration.

For DOI calibration, one reference detector and a ²²Na point source are normally needed. Traditional reference detector is consisted of a single crystal coupled to SiPM, which is placed on a precisely controlled movable platform to scan the whole length of crystal of the detector under test. To reduce the time length required for the calibration, our reference detector consists of a 16 × 16 LYSO crystal array, each with dimension of 1.6 × 1.6 × 10mm³ coupled to an 8 × 8 SiPM array. By arranging the test setup with geometric parameters as shown in Fig. 3, one quarter of crystal array can be scanned in one time of test without the movable platform involved. Considering the symmetry of the test detector, the DOI performance of the detector can be reflected by the test results of the quarter of detector. Depending on

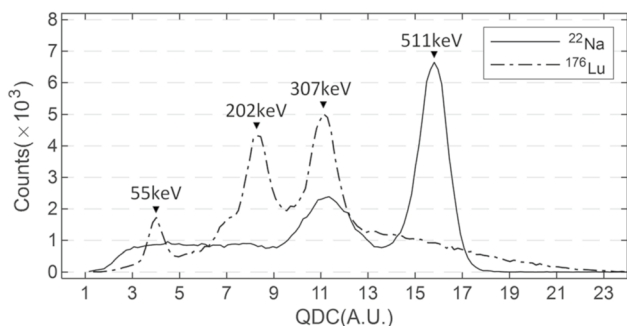


Fig. 2 Superposition of measured ¹⁷⁶Lu energy spectrum and ²²Na energy spectrum

Fig. 3 The schematic diagram of the setup for DOI calibration

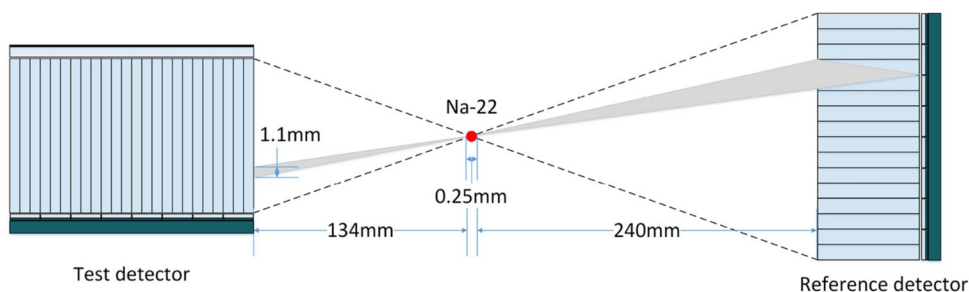
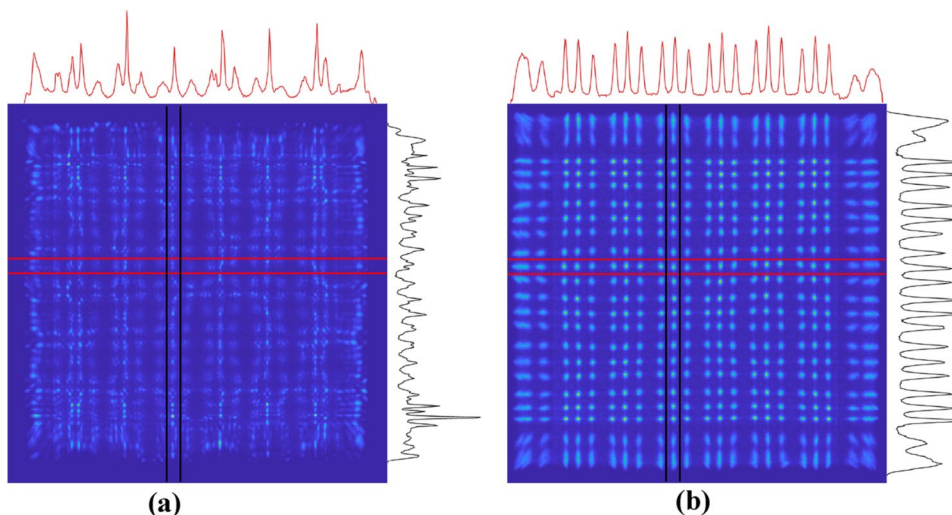


Fig. 4 Flood images with profile lines of 11th row and 11th column (a) without and (b) with energy calibration



the incident angle of the gamma ray, the incident beam size is different in different places inside of the test detector. According to the geometric distances of the setup along with the parameters of reference detector, the FWHM values of the beam size are ranging from 0.9 to 1.3 mm.

Results

Spatial resolution

Irradiated with a ²²Na source at distance of 150 mm, the flood image of the test detector is acquired. To show the benefit of energy calibration, the flood images together with profile lines of histogram of one row and one column without and with the energy calibration are compared as shown in Fig. 4. The crystal identification is significantly improved by the energy calibration. With the energy calibration, the spatial resolution of 1.0 mm can be achieved even for detectors with 9:1 coupling ratio.

Another interesting thing we found is that the average FWHM of peaks in profile lines in x direction (0.34 mm) is obviously smaller than that in y direction (0.41 mm), which can be attributed to the assembly process of the crystal array as shown in Fig. 5. For an N × N crystal array,

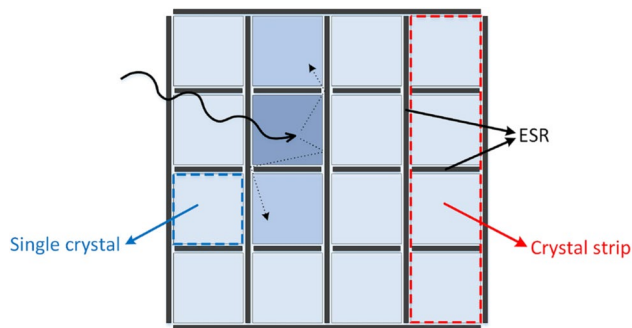


Fig. 5 Cross section of a 4 × 4 crystal array with different ESR separation

N independent single crystals are first glued together as a crystal strip with a narrow ESR inserted in between for light reflection. N crystal strips are then glued together to form an N × N crystal array with a large ESR inserted in between. Since the ESR size in the two direction is different, it is possible that a fraction of light can spread out to its neighbors in the strip direction, i.e., in y direction as shown in Fig. 5, which can slightly degrade the performance in the direction.

DOI capability

One column of the crystal array of the reference detector shown in Fig. 3 contains 16 crystals. We use the central 12 crystals to obtain 12 incident DOI positions with spacing of 0.94 mm in between. The distribution of the measured w at different depths z is plotted as shown in Fig. 6a, where the peak positions are obviously different at different z . The linear fitting between z and w for a crystal is shown in Fig. 6b. Using Eq. (5), the DOI resolution can be calculated from the measured FWHM value of w .

The measured DOI resolutions for all the crystals in the quarter of the detector to be tested are shown in Fig. 7. Since the outmost two rings of crystal cannot be separated clearly (Fig. 4b), the dotted lines are used to indicate that the two physically separate crystals (four crystals in the corner) are merged together as one unit to depict the performance. The DOI performance in the central part is relatively consistent, it turns worse toward the edge. In general, if the outmost two rings of crystal are not counted, the average DOI resolution in this central area is 4.1 mm, meanwhile the average DOI resolution of the whole detector is 4.7 mm.

We tried three kinds of light guides with thickness of 0 mm, 1 mm and 2 mm. We found there is a trade-off between DOI resolution and quality of flood image. The DOI resolution with 0 mm light guide is measured as 6 mm and it becomes better when we use thick light guides. However, the

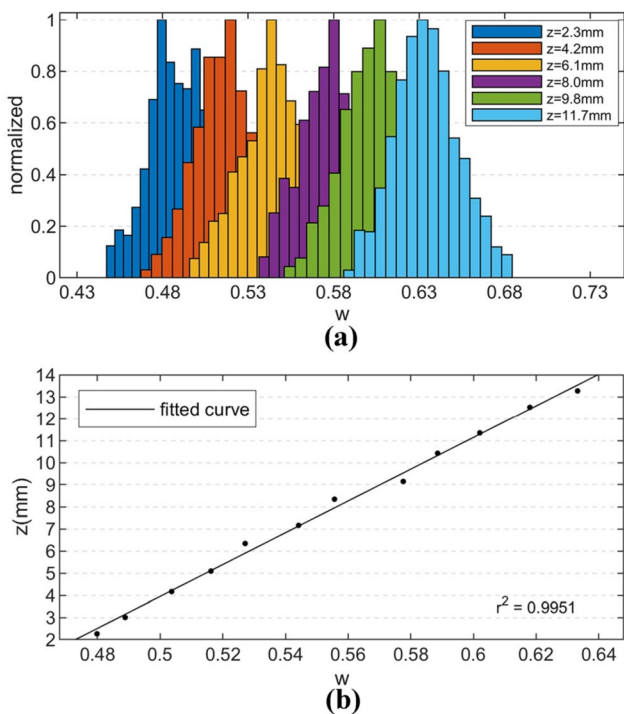


Fig. 6 a The distribution of w at different depths and b the relation between z and w of crystal (8, 17)

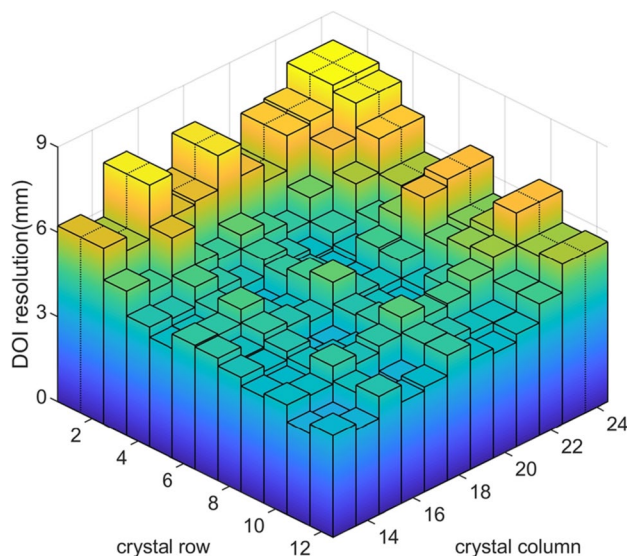


Fig. 7 The DOI resolution of a quarter of the test detector

equality of flood image becomes worse because more light is spread into other surrounding channels which spoils the flood image. Both the DOI resolution and the flood image are acceptable when we chose 1 mm light guide.

Energy resolution

In order to obtain the energy and timing performance of the detector, the setup was built including a coincident detector with the geometric parameters as shown in Fig. 8. The coincident detector is composed of an 8×8 LYSO crystal array, each with dimension of $3.36 \times 3.36 \times 10 \text{ mm}^3$ coupled to an 8×8 SiPM array. With the setup, the energy spectrum of all crystals in the detector can be acquired at the same time. Ignoring the DOI information, the original energy spectrum of crystal (17, 11), as shown in Fig. 9a, has an energy resolution of 18.0%. Because of the light attenuation along the crystal length, the events of same energy but with different DOI generate different readout values (QDC). The linear correlation between them is also observed as shown in Fig. 9b, which can be used for energy correction.

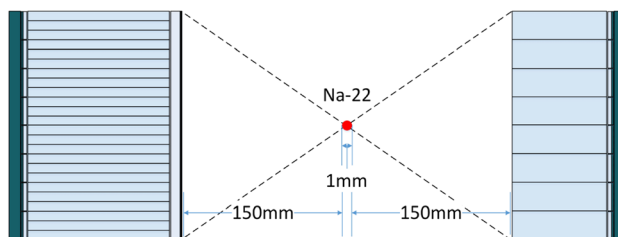


Fig. 8 Schematic diagram of the test setup for energy and time evaluation

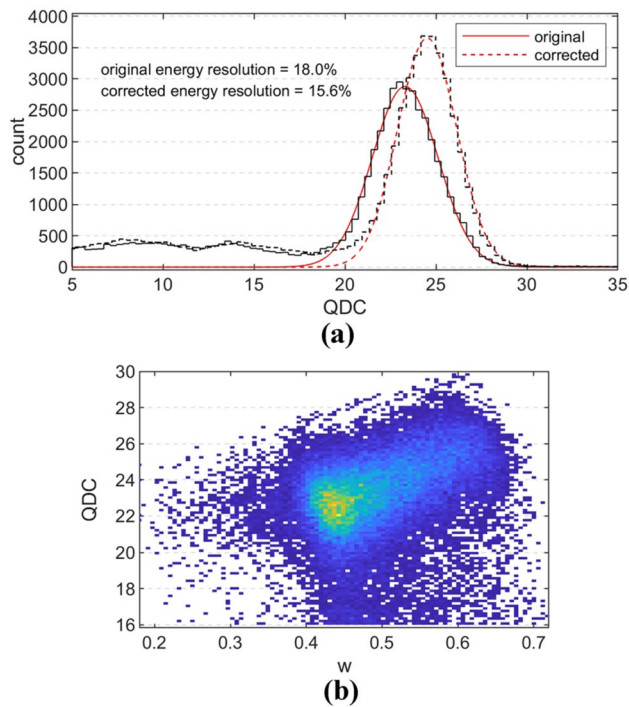


Fig. 9 **a** Energy spectrums before and after DOI correction and **b** scatter plot of TOFPET2 readout QDC versus DOI of crystal (17, 11)

The energy spectrum corrected by DOI information is also showed in Fig. 9a with the dotted line. The energy resolution is improved from 18.0 to 15.6%.

Since the outmost two rows (columns) of crystal cannot be clearly separated (Fig. 4b), these crystals, i.e., two crystals at edges and four crystals at corners are merged as one for energy spectrum acquisition. The energy resolutions of

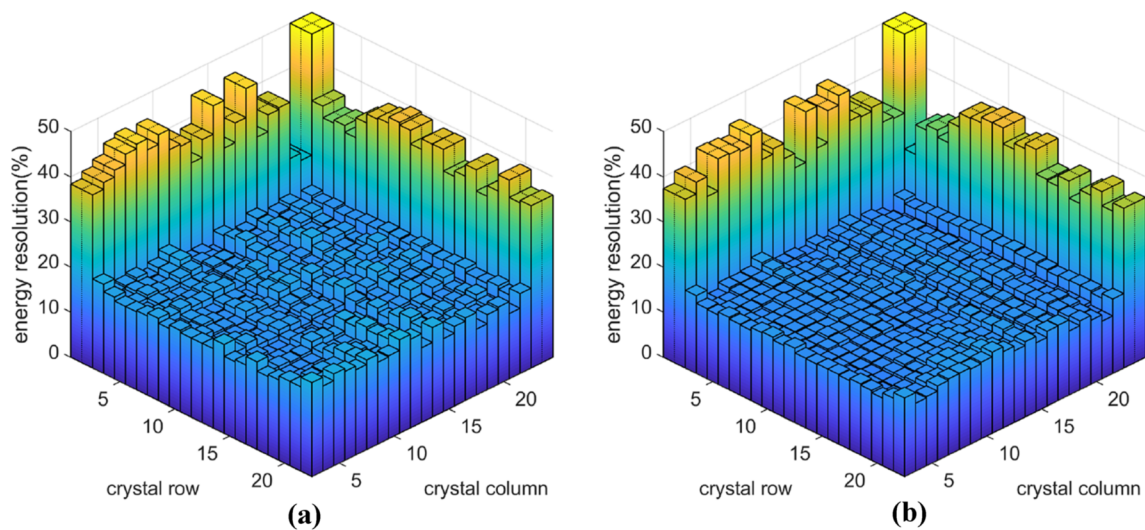


Fig. 10 Energy resolution of all crystals in the detector **a** before and **b** after DOI correction

all crystals in the detector before and after DOI correction can be compared as shown in Fig. 10, where the front two row and column were hidden just for easy viewing. After DOI correction, the average energy resolution is improved from 16.1 to 15.0% for central crystals, and 20.8–19.7% for whole detector.

Time performance

In order to obtain the time resolution of a channel in the coincident detector A, we used another two single-channel detectors B and C to measure the CTR of A + B, A + C and B + C, respectively. Therefore, the time resolution of the channel can be obtained. Repeating this process, the time performance of all the channels in the coincidence detector can be obtained. Using the known coincidence detector, the time resolution of the test detector in Fig. 8 can be determined, and then the CTR of two identical test detectors can be calculated. A typical relationship between w and the measured time difference is as shown in Fig. 11, where the peak position of time differences and the measured w has a linear relationship. The CTR between the two identical test detectors before and after the DOI correction are as shown in Fig. 12, where the average CTR is improved from 533 to 432 ps by the correction.

Conclusion

A high-resolution PET detector with depth encoding ability by using the light sharing and redirection method is developed and evaluated. Through the single-ended SiPM readout with commercialized TOFPET2 ASIC, the spatial

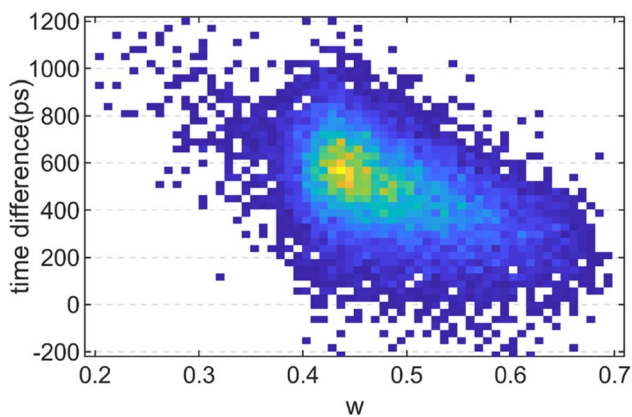


Fig. 11 Scatter plot of time difference versus w of crystal (17, 11)

the detector, the performance of the same detector but without the DOI capability, i.e., without the light guide at the top of crystal array, was also evaluated. The average energy resolution and CTR of this detector are 14.1% and 423 ps, respectively. Comparing with our DOI detector with 15.0% energy resolution and 432 ps time resolution, the DOI measurement does not deteriorate other properties of the detector. These test results show that the developed DOI detector is ready for practical for pre-clinical and organ-dedicated PET instrumentation.

resolution of 1.0 mm and DOI resolution of 4.1 mm can be obtained at the same time without increase the system complexity. As a comparison, the dual-end readout scheme using the same ASIC chip [18] can achieve better DOI resolution (2.33 mm) but with double complexity. Since the spatial and DOI resolutions depend on the light sharing, it is crucial that the readout has better linearity, which can be obtained by our proposed energy calibration method using LYSO background radiation. It is demonstrated that the spatial resolution can be significantly improved by the energy calibration, in particular for detectors with high coupling ratio between crystals and SiPM channels. In order to know whether the DOI measurement affects other properties of

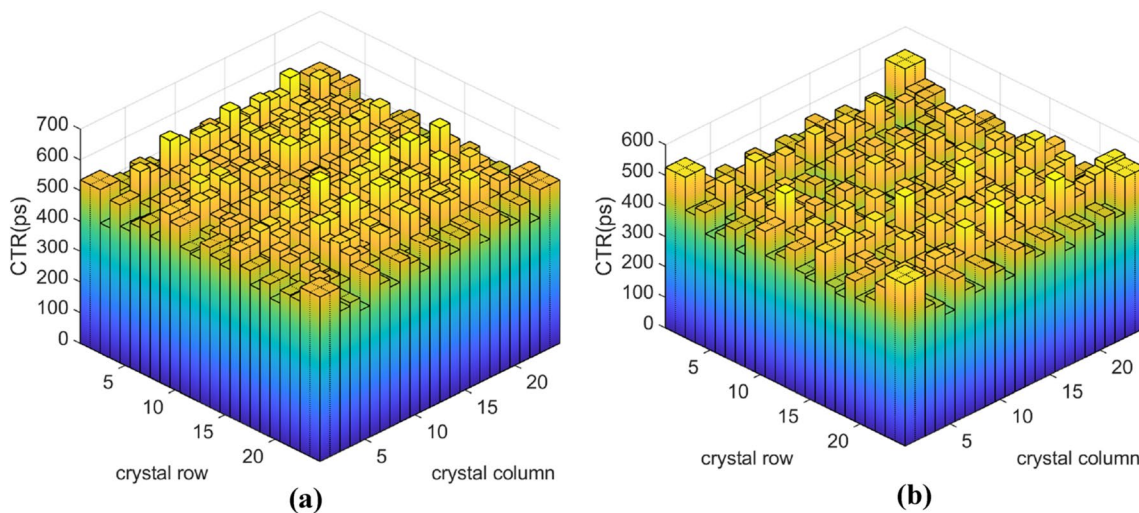


Fig. 12 CTR between two identical test detectors a before and b after DOI correction

Funding This work was supported by the National Natural Science Foundation of China [Grant Number 11735013].

Declarations

Conflict of interest On behalf of all authors, the corresponding author states that there is no conflict of interest.

References

1. A. Guerra and N. Belcari, Positron Emission Tomography: Its 65 years. (La Rivista del Nuovo Cimento 2016). <https://doi.org/10.1393/ncr/i2016-10122-6>
2. Z.H. Kuang et al., Performance of a high-resolution depth encoding PET detector using barium sulfate reflector. *Phys. Med. Biol.* **62**, 5945 (2017)
3. T. Liu, M. Niu et al., A ~0.7 mm Spatial Resolution All-digital Animal PET System using Improved Trans-PET Detectors. *NSS/MIC/RTSD 2016*
4. J. Du, X. Bai et al., Performance of a high-resolution depth-encoding PET detector module using linearly-graded SiPM arrays. *Phys. Med. Biol.* **63**, 035035 (2018)
5. Z.H. Kuang, X. Wang et al., Dual-ended readout small animal PET detector by using 0.5mm pixelated LYSO crystal arrays and SiPMs. *Nuclear Inst. Methods Phys. Res. A* **917**, 1–8 (2019)
6. W. Moses, Fundamental limits of spatial resolution in PET. *NIMA*, 2010.11.092.
7. H. Anger, Scintillation camera. *Rev. Sci. Instrum* **29**, 27 (1958)
8. Z. Kuang, Z. Sang et al., Development of depth encoding small animal PET detectors using dual-ended readout of pixelated scintillator arrays with SiPMs. *Med. Phys.* **45**(2), 613–621 (2018)
9. E. Yoshida, G. Hirumi et al., Four-layered DOI-PET detector with quadrisedected top layer crystals. *Nuclear Instrum. Methods Phys. Res Sect A: Accel. Spectrom. Detectors Assoc. Equip.* **933**, 1–7 (2019). <https://doi.org/10.1016/j.nima.2019.04.023>
10. B. Zhao, Z. Kuang et al., Depth encoding PET detectors using single layer crystal array with different reflector arrangements along depths. *Nuclear Instrum. Methods Phys. Res Sect A: Accel. Spectrom. Detectors Assoc. Equip.* (2019). <https://doi.org/10.1016/j.nima.2019.162600>
11. M. Pizzichemi, G. Stringhini et al., A new method for depth of interaction determination in PET detectors. *Phys. Med. Biol.* **61**, 4679–4698 (2016)
12. G. Stringhini, M. Pizzichemi et al., Development and evaluation of a practical method to measure the Depth of Interaction function for a single side readout PET detector. *2016 JINST 11 P11014*.
13. M. Pizzichemi, A. Polesel, et al., On light sharing TOF-PET modules with depth of interaction and 157ps FWHM coincidence time resolution. *Phys. Med. Biol.* (2019)
14. PETsys Electronics, Oeiras, Portugal, TOFPET2: a high-performance ASIC for time and amplitude measurements of SiPM signals in time-of-flight applications. www.petsyselectronics.com/web/
15. E. Lamprou, F. Sanchez et al., In-depth evaluation of TOF-PET detectors based on crystal arrays and the TOFPET2 ASIC. <https://doi.org/10.1016/j.nima.2020.164295>
16. L.W. Wang, Y.G. Wang, M.C. Wang, Energy calibration using scintillator background radiation for high-resolution PET detectors. <https://doi.org/10.1016/j.nima.2020.164202>
17. ON semiconductor application note, Linearity of the Silicon Photomultiplier. AND9776/D, Sep. 2018—Rev.2, www.onsemi.com
18. M. Li, S. Abbaszadeh, Depth-of-interaction study of a dual-readout detector based on TOFPET2 application-specific integrated circuit. *Phys. Med. Biol.* **64**, 108 (2019)